Large-scale synthesis of hybrid conductive polymer-gold nanoparticles using "sacrificial" weakly binding ligands for printing electronics.

Alberto Escudero,[1,2*] Lola González-García,[1] Robert Strahl[1], Dong Jin Kang[1], Juraj Drzic[1] and Tobias Kraus[1,3*]

[1]INM – Leibniz Institute for New Materials, Campus D2 2, 66123 Saarbrücken, Germany.

[2]Departamento de Química Inorgánica and Instituto de Investigaciones Químicas (IIQ), Universidad de Sevilla – CSIC, Calle Américo Vespucio 49, 41092 Seville, Spain.

[3]Colloid and Interface Chemistry, Saarland University, 66123 Saarbrücken, Germany.

*corresponding authors alberto.escudero@csic.es and tobias.kraus@leibniz-inm.de

Key words: gold nanoparticles, hybrid functional nanoparticles, high throughput synthesis, up-scaling, conductive ink, inkjet printing, printed electronics.

Abstract

We describe the gram-scale synthesis of hybrid gold nanoparticles with a shell of conductive polymer. A large-scale synthesis of CTAB-capped gold nanoparticles (AuNP@CTAB) was followed by ligand exchange with conductive polymers based on thiophene in a 10 L reactor equipped with a jacket to ensure a constant temperature of 40 ºC and a mechanical stirrer. Slow and controlled reduction of the gold precursors and the presence of small amounts of silver nitrate are revealed to be the critical synthesis variables to obtain particles with a sufficiently narrow size distribution. Batches of approximately 10 g of faceted AuNP@CTAB with tunable average particle sizes from 54 to 85 nm were obtained per batch. Ligand exchange with PEDOT:PSS in the same reactor then yielded hybrid Au@PEDOT:PSS

nanoparticles. They were used to formulate sinter-free inks for the inkjet printing of conductive structures without the need of a sintering step.

1. Introduction

Hybrid nanoparticles (NPs) consisting of an inorganic core and an organic shell combine the functionality of both.[1-2] In particular, within the field of printing electronics, films of hybrid NPs consisting of a gold core coated with conductive polymers achieve conductivity directly after deposition from liquid dispersions and drying at room temperature. The presence of the conductive organic polymer shell on the Au surface provided not only colloidal stability at high NP concentrations (around 200 mg of Au per mL), but also good electron transport properties in dry state.[3] Such properties pave the way for the applications of hybrid Au NPs in flexible printing electronics, through the production of inkjet printing sinter-free inks, thus offering a low material amount demanding technology and a potential use on soft substrates.

Many different strategies are reported for the synthesis of hybrid NPs,[4-5] and the synthesis process of conductive hybrid gold NPs is well established at laboratory scale.[3] Processes that yield quantities sufficient for the preparation of macroscopic materials, or at least macroscopic areas of thin films, have been studied much less, however. Synthetic routes for larger amounts of hybrid NPs with controlled NP sizes and morphologies that ensure colloidal stability are lacking. It is particularly difficult at present to obtain larger quantities of high-quality metal NPs with weakly bound ligands that are suitable for later ligand exchange steps.

The scale-up of metal NP synthesis is possible by increasing the synthesis volume[6-7] and/or the metal precursor concentrations, or by separating the synthesis into sequential growth steps.[8] The use of higher precursor concentrations usually imply the use of strongly binding ligands that can control the particle size and morphology even for imperfect mixing in large volumes and stabilize the dispersion during and after the synthesis at high particle concentrations.[9-10] Syntheses carried out in organic solvents enable the use of higher precursor concentrations, but lossy phase transfer steps are required to create aqueous

dispersions.[11] This leads to a dilemma in the production of hybrid NPs: on one hand, the desired functional ligand might not lead to the desired core shape and size while, on the other hand, the use of strongly bonded ligands hinders its replacement for a functional shell in a sequential process of ligand exchange.

One may consider two synthetic strategies to resolve this dilemma. A one-pot approach that yields hybrid particles in a single step would avoid the need for weakly binding ligands and avoid their limitations altogether. As an alternative, we may seek "sacrificial" ligands that bind strong enough to enable an (optimized) synthesis but can still be replaced in a subsequent step. While the first approach has the advantage of producing the hybrid particles in a single step, it requires the *ad hoc* design and optimization of each hybrid particle synthesis. The second strategy makes it possible to use the same inorganic cores for different hybrid particles if the sacrificial ligand can be replaced. The challenge is, then, to reliably prepare high-quality nanoparticles in sufficient quantities using a rather labile ligand. This contribution demonstrates the feasibility of the approach for a specific case of hybrid particles.

In this paper, we present an aqueous synthesis of ≈10 g per batch gold NPs with a good control of their size and morphology with a subsequent ligand exchange to create electrically conductive hybrid particles with a total yield of 83 %. Synthesis involves two steps: (i) reduction of gold in order to obtain NPs with morphology-directing "sacrificial" ligand, and (ii) a ligand exchange with the functional semiconductor polymer ligand. Hexadecyltrimethylammonium bromide (CTAB) was selected as the sacrificial capping agent to first synthesise AuNP@CTAB. It is known that CTAB can control metal NP size and shape;[2, 12] the CTAB shell provides colloidal stability to growing particles at high precursor concentrations through steric stabilisation.[13-15] After synthesis, CTAB can be replaced at mild conditions by many different ligands.[16-18] as we recently demonstrated at the laboratory scale with conductive polymers based on thiophenes.[3] The conductive poly(3,4-

ethylenedioxythiophene) polystyrene sulfonate (PEDOT:PSS) was selected as the functional ligand to create hybrid NPs. It confers the hybrid NPs high long-term colloidal stability in dispersion at high NP concentration (20 - 25 wt.%) and provides them with electrical conductivity in the dried state.[3] These two characteristics are desired, for instance, for the formulation of inks for inkjet printing in the field of printed electronics,[19] avoiding aggregation and block of the nozzles, and allowing electrical conductivity without the need of any further treatment.

For the first step, we optimized the widely used seed-mediated strategy of Ye and co-workers,[20] which used laboratory ovens and standard laboratory glass materials. We obtained amounts above 1 g of monomodal AuNP@CTAB per synthesis in a 1 L reactor equipped with a jacket to control the temperature and a mechanical stirrer, and were able to tune the average diameter (± standard deviation) from 54 ± 15 to 85 ± 9 nm at reaction yields between 85 and 90% (section 3.1). The synthesis took place at 40 ºC and did not require additional growth steps. We studied the effects of the reagent concentrations, gold reduction rate, and seed concentration on the NP size, morphology, and width of the particle size distribution in order to maximize the gold precursor concentration and thus, the amount of particles obtained per batch. Reaction conditions were first optimized in a continuously stirred 1 L reactor. The synthesis was then scaled linearly by increasing volume and the reagent amounts by a factor of 10 (section 3.2). The scaled process yielded amounts higher than 10 g of NPs per batch, and the particle quality was very close to the 1 L batches. A proposed nanoparticle formation mechanism under such synthetic conditions is discussed in section 3.3.

The exchange of the sacrificial ligand for a functional polymer was performed in the same reactor after purification of the particles. We replaced CTAB with the conductive polythiophene PEDOT:PSS. Ligand exchange at room temperature and suitable PEDOT:PSS concentration ensured good colloidal stability and yielded a high-quality dispersion of

hybrid AuNP@PEDOT:PSS (section 3.4). Highly concentrated, aqueous dispersions of conductive hybrid NPs were finally inkjet printed on different substrates to create conductive structures (section 3.5) in order to demonstrate the applicability of the scaled synthesis.

2. Experimental section

2.1 Materials

Tetrachloroauric (III) acid trihydrate ($HAuCl_4 \cdot 3H_2O$, Acros Organics, #411070259) was selected as gold precursor. Hexadecyltrimethylammonium bromide (CTAB, Sigma-Aldrich, >99%, #H6269, a single 1 kg package was used for all 1 L syntheses and two separate 1 kg batches for the 10 L syntheses), sodium oleate (Sigma-Aldrich, >82% fatty acids, #26125), silver nitrate ($AgNO_3$, Honeywell, 99.0%, #209139), sodium borohydride ($NaBH_4$, Sigma-Aldrich, >98.0%, #452882), L-ascorbic acid (Sigma-Aldrich, #A0278) were used for the synthesis of the particles. The commercial PEDOT:PSS dispersion Clevios P (Heraeus, 1.3 wt%) was used for the ligand exchange. All the chemicals were used as received without further purification. Double reverse osmosis water (i.e. ultrapure water, conductivity ~ 3 µs/cm) was used for all the synthesis, ligand exchange and cleaning steps. Concentrated dispersion of the hybrid nanoparticles were finally prepared in Millipore water.

2.2 Large-scale synthesis of AuNP@CTAB

Samples with different gold precursor and additive concentrations were prepared as shown in Table 1. The synthesis was first scaled to 1 L, parameters were optimized, and the process was scaled linearly to a 10 L reactor, as described below. Both the 1 L and the 10 L reactors (HWS, Mainz, Germany) were made out of 3.3 borosilicate glass and were equipped with a jacket to control the temperature and a RW20 DZM (1 L) and RW 25 (10 L) mechanical stirrer (IKA Labortechnik, Staufen, Germany). Images are shown in Figure S1. The synthesis

was based on a seeded growth strategy. A gold precursor ($HAuCl_4$) was slowly reduced with ascorbic acid in the presence of preformed gold seeds, CTAB, sodium oleate, and silver nitrate. It was not necessary to clean the reactor with aqua regia; simple cleaning with ultrapure water and laboratory paper proved sufficient.

Table 1: Samples and reaction conditions used in the 1 L (Au1 to Au8 samples) and the 10 L (A9 and A10 samples) reactor. The ascorbic acid concentrations always refer to 25 mL of the solution, added at 1.3 mL/h. (*) = uncontrolled addition of ascorbic acid (fast addition of 2 mL of the solution every 2 min). NaOL = sodium oleate.

Sample	$HAuCl_4 \cdot 3H_2O$ [mM]	CTAB [mM]	NaOL [mM]	$AgNO_3$ [μM]	Ascorbic acid [mM]	Seeds [mL]	Particle size [x±σ, nm]
Au1	4.6	60.2	8.9	110	64 (*)	9.4	Approx. 1000
Au2	4.6	60.2	8.9	110	64	9.4	85 ± 9
Au3	4.6	60.2	8.9	110	64	18.7	Polydisperse
Au4	4.6	120.4	17.8	110	64	18.7	75 ± 7
Au5	4.6	120.4	17.8	1655	64	18.7	54 ± 15
Au6	4.6	60.2	8.9	0	64	9.4	Polydisperse
Au7	7.9	120.4	17.8	1655	109.4	32	87 ± 14
Au8	12.6	120.4	17.8	2648	175.0	51.2	Polydisperse
Au9-10L	4.6	120.4	17.8	110	650 (0.6 mL/h)	190	77 ± 8

Au10-10L	7.9	120.4	17.8	1655	1100 (0.6 mL/h)	270	71 ± 29
Au9-10L-LE	Ligand exchange with PEDOT:PSS of sample Au9-10L						
Au10-10L-LE	Ligand exchange with PEDOT:PSS of sample Au10-10L						

2.2.1 Synthesis of the gold seeds: 90 mL of an aqueous 0.5 mM $HAuCl_4 \cdot 3H_2O$ solution (17.7 mg) were added to 90 mL of an aqueous 0.2 M CTAB solution (6.56 g CTAB) in a glass vial under mechanical stirring. Afterwards, 10 mL of a 6.9 mM $NaBH_4$ aqueous solution were added to the vial. The stirring was kept for 90 seconds and the sample was aged without stirring for 30 additional minutes at 40 ºC, resulting in a dispersion of the gold seeds. It is important to note that the $NaBH_4$ should be freshly prepared before seed synthesis. To do so, 26 mg of $NaBH_4$ were dissolved in 10 mL of ultrapure water, and 1 mL of this solution was later added to a vial containing 9 mL of ultrapure water, resulting in 10 mL of a 6.9 mM $NaBH_4$ solution. A particle size around 4 nm has been reported in the literature for similar protocols performed with smaller reaction volumes.[14] Up to at least 270 mL of seed solution can be produced by increasing the volume of the reactant solutions with the same concentrations. All the seeds employed in this work were freshly prepared.

2.2.2 Synthesis of the AuNP@CTAB in a 1 L reactor: We describe the synthesis process using the amounts used for the Au4 sample (conditions for the other samples are indicated in Table 1). First, 35.1 g of CTAB and 4.36 g of sodium oleate were added to 751 mL of ultrapure water, and were dissolved with the help of a 150 rpm mechanical stirring at 45-50 ºC. After approximately 20 min, a clear solution was obtained, the temperature was set at 40 ºC, and a solution of 15 mg of $AgNO_3$ in 20 mL of ultrapure water was added. Afterwards, 1.46 g of $HAuCl_4 \cdot 3H_2O$ previously dissolved in 8.5 mL of ultrapure water were added. This solution was aged at 40 ºC until a light yellow colour appeared, and it was

ensured that the precursor had fully dissolved (which was the case after approximately 1 h). Then, 18.7 mL of the seed solution were added. Finally, 25 mL of ultrapure aqueous 64 mM ascorbic acid (corresponding to 286 mg of ascorbic acid) were introduced into the reaction at a controlled speed of 1.3 mL/h. The solution was continuously stirred at a speed of 150 rpm in order to have an homogenious mixture. The reaction colour changed from light yellow – transparent to light pink and eventually to brown, and was left overnight. (approx. 19 hours). We confirmed that all the gold precursor was reduced to Au (0) by removing small aliquots of the suspension, centrifugation of the aliquot, and analysis of the supernatant. If the addition of a small amount of $NaBH_4$ to the supernatant did not change the colour, we assumed that all gold ions had been reduced.

The resulting dispersion of gold nanoparticles (approx. 825 mL) was transferred into one 1.5 L centrifuge tube and diluted with ultrapure water to fill the tube, yielding a CTAB concentration of approximately 66 mM for samples Au4, Au5, and Au7. Centrifugation in a Sigma 8k centrifuge at 8578 rcf for 1 h separated the particles from supernatant. Note that higher centrifugation speeds may lead to nanoparticle aggregation and, in some cases, coalescence. Centrifugation was repeated two times. We removed approximately 90% of the supernatant after the first centrifugation step and added fresh ultrapure water to reach a CTAB concentration of approximately 6.6 mM. As much as possible of the supernatant was removed after the second centrifugation step, and the remaining dispersion was transferred to one standard 50 mL tube, which was additionally centrifuged once in a Hettich Universal 320L centrifuge at 6420 rcf for 45 min. As much as possible of the supernatant was removed and the AuNP@CTAB were finally dispersed in around 11 mL of 5 mM CTAB.

2.2.3 Synthesis of the AuNP@CTAB in a 10 L reactor: All liquid reagent volumes used in the 1 L synthesis were increased by a factor of 10 at constant concentrations. Exemplary reaction sequences for samples Au9-10L and Au10-10L are given in Figure 1. The procedure for batch Au9-10L was as follows: 351 g of CTAB and 43.6 g of sodium oleate were dissolved

in 7900 mL of ultrapure water with the help of mechanical stirring (150 rpm) for approximately 20 min at 45 – 50 ºC. The temperature was then reduced to 40ºC, and 145 mg of $AgNO_3$ (dissolved in 10 mL of water), 14.6 g of $HAuCl_4 \cdot 3H_2O$ (dissolved in 85 mL of water) were added to the solution. All solids had fully dissolved after one hour. We then added a volume of 190 mL of the fresh seed solution (section 2.2.1). Immediately afterwards, 25 mL of 6.4 mM ascorbic acid (2.87 g) were added to the reaction at 0.6 mL/h, and the reactor was stirred at 150 rpm in order to have a homogeneous mixture for 42 h.

The resulting dispersions were transferred into six 1.5 L centrifuge tubes and the NPs were purified by centrifugation (Sigma 8k centrifuge, 8578 rcf, 1 h) for three times. We removed approximately 90% of the supernatant (with a starting CTAB concentration of 120.4 mM) after the first centrifugation step and added fresh ultrapure water to achieve an approximate CTAB concentration of 12 mM. Half of the supernatant was removed after the second centrifugation step to reach a final CTAB concentration of around 6 mM. After the third centrifugation step, as much supernatant as possible was removed. The AuNP@CTAB were finally dispersed in 250 mL of aqueous 5 mM CTAB solution for storage. Samples of 1 mL were taken from the reactor directly after synthesis and analyzed by TEM. They were prepared for microscopy by centrifugation in a small eppendorf centrifuge (4000 rpm, 5 min) to remove solutes, dried on TEM grids, and observed. We found particle morphologies and sizes that were indistinguishable from those in the final product of the overall process.

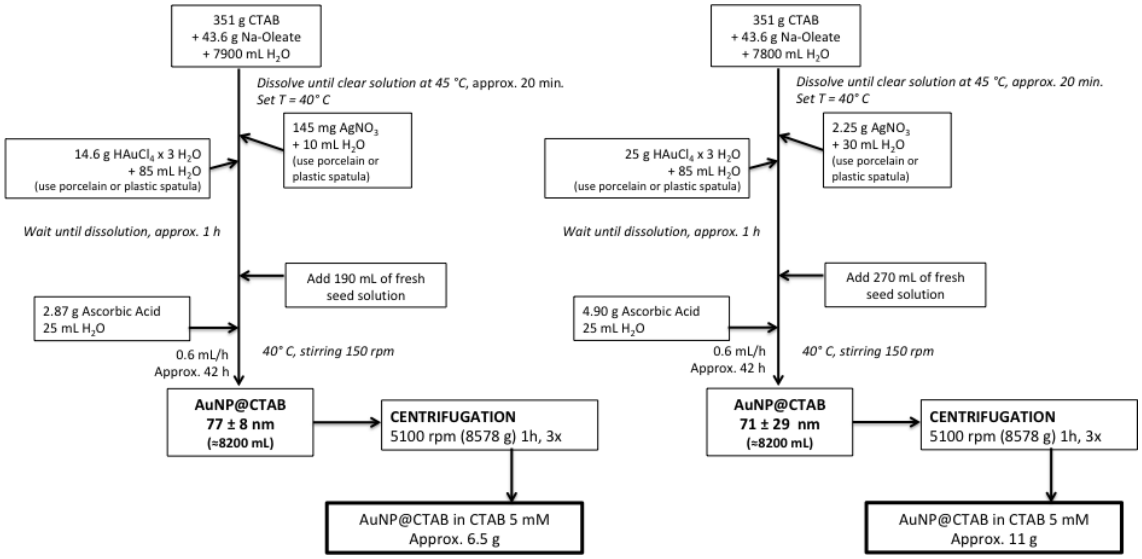

Figure 1: Reaction flows of the AuNP@CTAB synthesis carried out in a 10 L reactor, corresponding to the Au9-10L (left) and Au10-10L (right) samples.

2.3 Ligand exchange with PEDOT:PSS

We report the conditions for the ligand exchange of the sacrificial CTAB by PEDOT:PSS in the 10 L reactor. This protocol can also be applied in the 1 L reactor by linear downscaling. The final dispersion of Au@CTAB obtained from the synthesis and purification discussed above was prepared as discussed below and added to an aqueous suspension of Clevios P (PEDOT:PSS) at a mass ratio AuNP@CTAB : PEDOT:PSS of 1 : 0.8, and a residual CTAB concentration of 80 µM. Both the CTAB concentration and the incubation time were chosen based on literature reports to ensure complete exchange of the ligand.[3, 21] Exemplary reaction numbers are given for sample Au9-10L-LE, obtained from sample Au9-10L that was synthesized in a 10 L batch. The sample was concentrated from 250 to 110 mL by centrifugation and removal of the appropriate supernatant volume (Hettich Universal 320L centrifuge, 6420 rcf, 45 min). The resulting concentrated dispersion in 5 mM CTAB was then added to a dispersion of 405 g of Clevios P in 7800 mL of ultrapure water, leading to a residual CTAB concentration of 80 µM. The mixture was left overnight (approx. 18 h) under mechanical stirring (150 rpm) at room temperature. The dark colour of the PEDOT:PSS

dispersion did not change appreciably during the ligand exchange. The NP dispersion was transferred into six 1.5 L centrifuge tubes after these 18 h. Excess reagent was removed by centrifugation in a Sigma 8k centrifuge at 8578 rcf for 1 h. The maximal possible amount of the supernatant was removed, ultrapure water was added to fully refill the tubes, and the suspensions were sonicated. Centrifugation was repeated three times, and the remaining suspension was dispersed in 250 mL of Millipore water. The dispersion was filtered with a Titan 3 1.5 μm nylon-based filter (Thermo Scientifics) to remove larger particles and finally concentrated in a Hettich Universal 320L centrifuge (5500 rcf, 1 h) to a final volume of 27 mL, giving rise to a concentrated dispersion of hybrid NPs of an approximate concentration of 200 mg Au/mL. The overall process at the 10 L scale required 3.5 days for all the synthesis and purification steps. We found 2.5 days sufficient for the 1 L reactor.

2.4 Nanoparticle characterization

Particle morphology and composition was examined by scanning electron microscopy (SEM, FEI Quanta 400 ESEM, FEG, Germany, equipped with an EDAX Genesis V6.04 X-ray spectrometer and operating at 10-20 kV. For quantification of the elemental composition, Energy-dispersive X-ray (EDX) spectra were collected with an acquisition time of 1000 s, and the AuL and AgL lines were used after ZAF correction. Some samples were also analyzed by transmission electron microscopy (TEM, JEM2010, JEOL, Japan) operating at 200 kV. The samples were dispersed in water, sonicated and dropped on either a silicon wafer (for SEM analysis) or a conventional carbon-coated copper grid (for TEM analysis). Particle size distributions were obtained by counting approximately 100 particles on both the SEM and TEM micrographs and manually measuring their diameters in the images. Dynamic light scattering (DLS, Malvern Nano ZSP Zetasizer, laser wavelength 632.8 nm) was used to obtain the size distribution of the NP suspensions in water at pH 6.5 by using a distribution algorithm, and the mean hydrodynamic diameters (Z average, defined as the intensity weighted mean hydrodynamic size of the ensemble collection of particles assuming a single

particle size a single exponential fit) were obtained using a distribution and a cumulant fit, respectively. The Zeta (ζ) potentials of NP suspensions in water at pH 6.5 were measured in the same setup using Doppler-based electrophoresis analysis. The gold concentrations of the resulting suspensions were assessed by induced coupled plasma atomic emission spectroscopy (ICP-AES) using an ICP Horiba Jobin Yvon ULTIMA2 spectometer, for which the gold NPs were dissolved in aqua regia. Optical characterization of the dispersions was performed with a UV-vis/NIR spectrophotometer (Cary 5000, Varian, CA, USA) in absorbance mode. The viscosity of the hybrid NP suspensions was measured with a Discovery HR-3 (TA Instruments, New Castle, USA) device.

2.5 Inkjet printing of conductive structures on glass, PET foil and other substrates, and characterization

An aqueous dispersion of AuNP@PEDOT:PSS with a concentration of 200 mg/mL was obtained from sample Au9-10L-LE as described above. We used the resulting dispersion directly as an ink in a drop-on-demand (DOD) inkjet-printing platform (PiXDRO LP50 from Meyer Burger). The LP50 is a high precision inkjet printer with 5-axis motion and an accuracy of < 20 µm (3σ), < 5 µm (3σ) repeatability. A Dimatix Materials Cartridge DMC11610 from FujiFilm was employed as print head. It is a piezo-driven jetting device with 16 nozzles and 254 µm spacing in a single row that ejects drops with a nominal volume of 10 pL. Prior to printing, the dispersion was filtered with a 0.22 µm hydrophilic PES filter (Carl Roth).

We printed using a custom voltage profile to drive the Piezo print head. A trapezial waveform from 2 V up to 7 V filled the ink chamber. A short peak interjected in the centre of the trapezoid, where the voltage reaches 21 V was used to eject the droplet. The head moved at a speed between 100 – 150 mm/s and deposited droplets at a density of 2000 dpi. This configuration let us to create lines with widths down to 30 µm. Their geometries were characterized by means of optical microscopy (Zeiss Scope.A1) for the width (*W*) and length

(L). The thickness (t) was measured by confocal microscopy using a MarSurf CM explorer (Mahr GmbH, Germany).

The electrical characterization of the printed paths on glass was performed using 2-point-probe configuration to acquire the current-voltage (I-V) curves with a Keithly 2450 source meter at room temperature. The specific resistivity (ρ) was calculated with the obtained resistance (R) from the I-V curves and the equation 1:

$$\rho = R \cdot \frac{W \cdot t}{L}$$

(equation 1)

Nine samples were characterized to give the average value and its standard deviation.

3. Results and discussion

Gram-scale amounts of hybrid AuNP@PEDOT:PSS with controlled size and morphology were obtained by synthesising AuNP@CTAB and ligand exchange with the conductive polymer PEDOT:PSS. Section 3.1 analyses the reaction parameters that yielded large amounts of uniform AuNP@CTAB in the 1 L reactor. The optimized reaction conditions were scaled to 10 L batches (section 3.2) The proposed reaction mechanism of the AuNP@CTAB at such experimental conditions is explained in section 3.3. The production of hybrid AuNP@PEDOT:PSS by ligand exchange in the 10 L reactor is described in section 3.4. Finally, we discuss how such hybrid particles can be used for inkjet printing of conductive structures (section 3.5).

3.1 Upscaling AuNP@CTAB synthesis at the 1 L scale

The objective was to synthesize large amounts of uniform, isometric AuNP@CTAB at increased quantities by both increasing precursor concentrations and reaction volume. The starting point of the scale-up was the synthesis protocol by Ye et al.[20] that the authors performed in a 1L Erlenmeyer flask, at gold precursor concentrations around 0.5 mM and

reaction volumes up to 0.5 litres, values that are typical for the laboratory scale synthesis of Au NPs in general.[14, 20, 22-24] Upscaling such processes involves changing the reactor type, which will often change the kinetics of the reaction[25] and affect particle size and morphology. Linear scaling of experimental parameters such as reagent volume does not always retain particle quality. We therefore optimized the conditions in a 1 L stirred reactor in order to obtain a protocol that could be directly scaled to 10 L.[26] The gold precursor concentration and the amount of added ascorbic acid was increased to obtain larger amounts of NPs, the amount of added seeds was increased to decrease the mean NP size. Other parameters such as the addition of $AgNO_3$ and the CTAB concentration were varied in order to obtain optimal AuNP qualities. Note that sodium oleate slowly reduces Au (III) to Au (I), visible through the disappearance of the orange–yellow color.[20] We employed a ratio of ascorbic acid : $HAuCl_4$ that was slightly above unity to ensure complete reduction of Au (I) to Au (0), which it is known to be also catalysed by gold seeds.[27]

For the synthesis carried out in the 1 L reactor, we increased the concentration of $HAuCl_4 \cdot 3H_2O$ to 4.6 mM and increased the volume of both the gold seed dispersion and ascorbic acid solution by a factor of 10, proportional to the increase in the gold precursor concentration. The pH of the reaction was not adjusted using HCl as in the original protocol, because any addition of HCl decreased particle quality.

We investigated the influence of the addition rate of the reducing agent (ascorbic acid) into the reaction mixture on the particle morphology. Increased gold precursor concentrations can provoke a rapid, localized reduction of gold ions when the reducing agent is added, which leads to inhomogeneous nucleation and/or a locally faster particle growth and thus, wide and even multimodal particle size distributions. Moreover, the amount of ascorbic acid, the details of its addition, and the exact reaction times have been identified as factors of surface reconstruction that affect the binding of surfactants and thus, the final morphology of the particles.[28-29]

For the synthesis in the 1 L reactor, we tested a fast, stepwise addition of 64 mM ascorbic acid solution by rapidly adding aliquots of 2 mL per minute and obtained particles with diameters of around 1 µm that seemed to be aggregates of smaller units (Sample Au1, Figure 2A). The slow addition of ascorbic acid solution with a syringe pump at a flow rate of 1.3 mL/h under the same conditions produced homogeneous and faceted particles with a mean diameter of 85 nm and a standard deviation of 9 nm according to SEM micrographs (Sample Au2, Figures 2B and 2C). Note than while CTAB-based routes are often associated with gold nanorods, other particle morphologies have been reported in the literature, depending on the concentrations of the seed particles, CTAB, and the reactants Au^{3+} and ascorbic acid.[30] The reaction conditions used here are characterized by high gold precursor concentrations that likely provoke a thermodynamically controlled growth and thus, isometric nanoparticle morphology. Comparable syntheses with gold precursor concentrations of 1 - 2 mM have yielded thermodynamically stable crystal facets,[8] isotropic particle shapes,[31] and isometric gold NPs,[32] in good agreement with our observations.

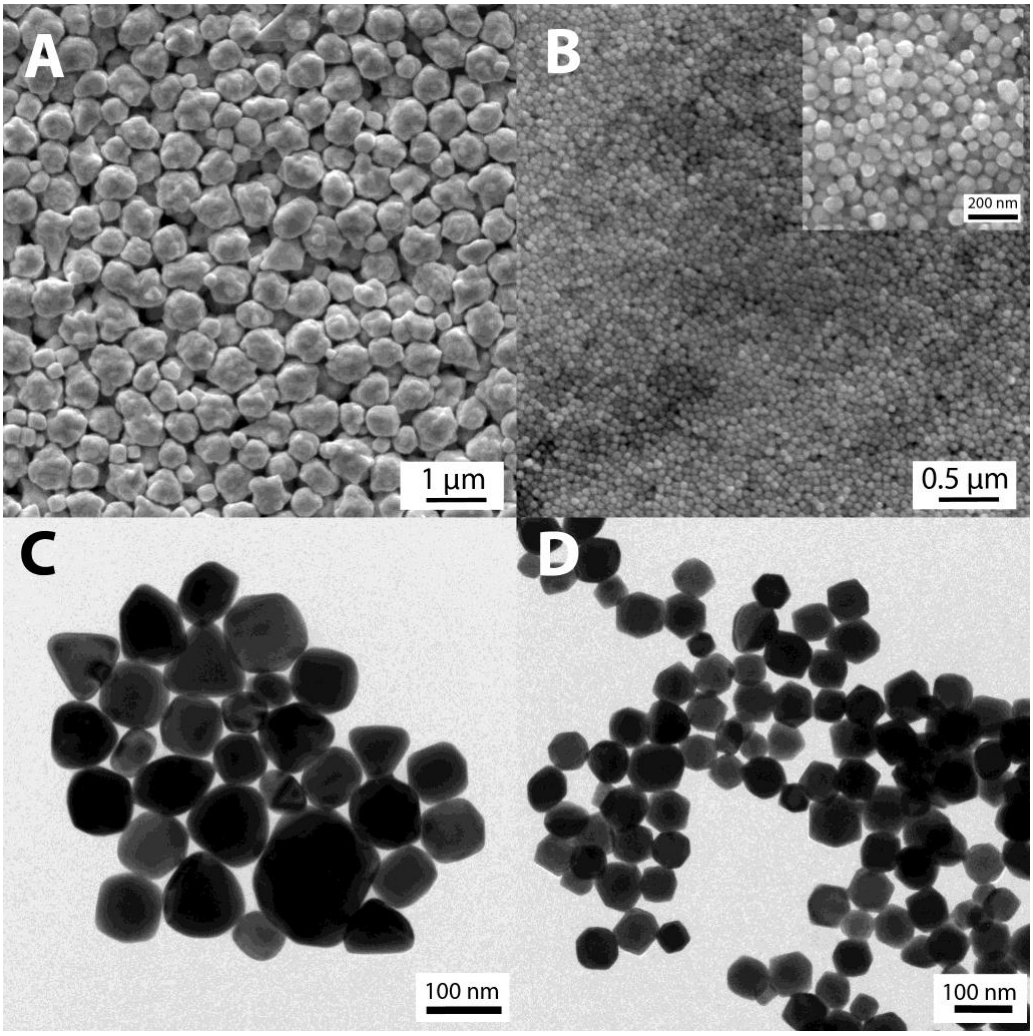

Figure 2: Scanning electron micrographs of particles from (A) sample Au1 with a fast and stepwise addition of ascorbic acid and (B) sample Au2 with a controlled and slow addition of ascorbic acid. Slow addition reduced the particle size, improved homogeneity and reduced the width of the size distribution. Transmission electron micrographs of the samples (C) Au2 and (D) Au4 show the reduction in the particle size when increasing the CTAB and sodium oleate concentrations as well as the amount of added seeds. The reaction conditions for each sample are shown in Table 1, experimental section.

In general terms, slow and controlled nucleation and/or growth and/or precipitation processes are required to obtain homogeneous particles.[33-34] In our case, the slow addition of ascorbic acid probably slows the reduction of Au cations down and promotes the

deposition of gold onto the growing Au seeds, avoiding localized secondary nucleation even in concentrated mixtures.

The second variable that we optimized was the amount of seed particles. Increasing the number of seeds reduce the particle size in an idealized seed-mediated synthesis,[6] enabling the desired control of average particle diameter,[35-37] but secondary effects such as agglomeration or imperfect mixing can impede this approach. We doubled the amount of seeds by adding twice the seed dispersion volume while keeping all other reaction variables constant and obtained particles with larger average diameters and a wider size distribution (Sample Au3, Figure 3A). Increasing both the number of added seeds and the CTAB and sodium oleate concentration produced more homogeneous particles with an average diameter of 75 nm and a standard deviation of 7 nm (Sample Au4, Figure 2D). We conclude that scaling via gold precursor concentration requires a proportional increase in the amount of gold seeds, and that the particle size can be reduced by both adding more seeds and increasing the CTAB and sodium oleate concentration, which may be connected to the stability of the seeds at increased gold precursor concentrations.

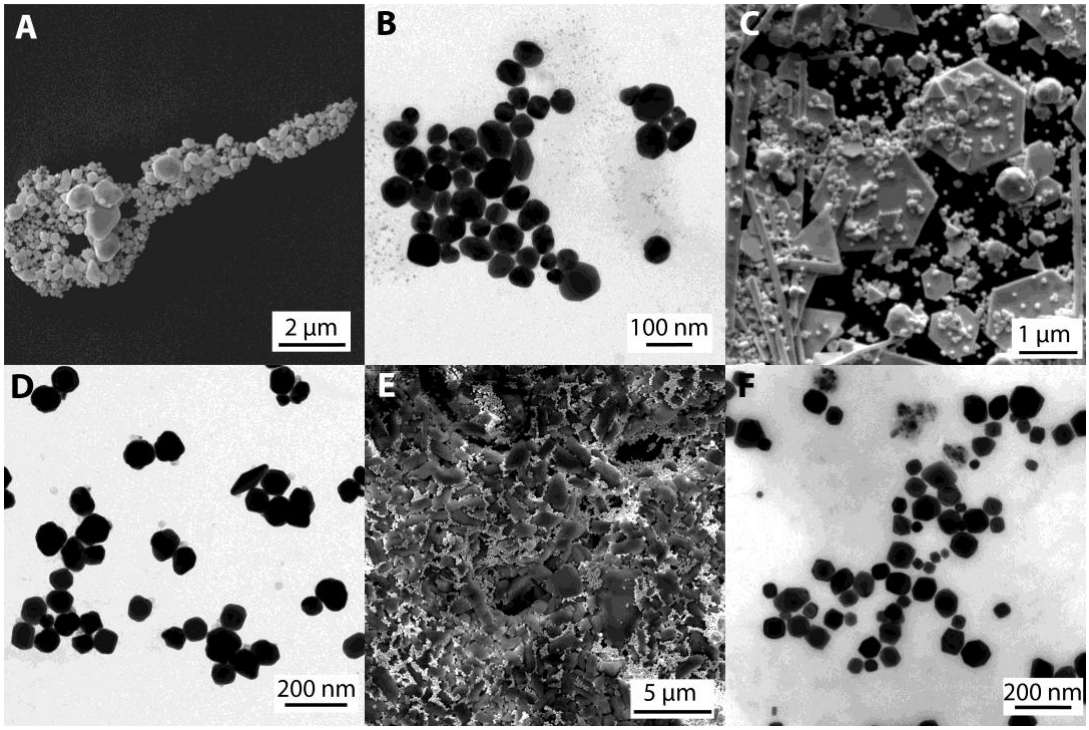

Figure 3: Representantive scanning and transmission electron micrographs of particles from the samples (A) Au3, showing how increasing the amount of added seeds without changing both CTAB and sodium oleate concentrations results in larger NPs with a wider size distribution; (B) Au5, indicating how incrased concentrations of $AgNO_3$ give rise to smaller NPs; (C) Au6, showing how the absence of $AgNO_3$ produces larger and polydisperse particles; (D) Au7, demonstrating how enhanced $HAuCl_4$ concentrations (7.9 mM) combinated with higher concentrations of $AgNO_3$ (1655 µM) result in homogenious AuNP@CTAB; (E) Au8, indicating how a $HAuCl_4$ precursor concentration of 12.6 mM results in polydisperse particles; and (F) Au10-10L, which corresponds to AuNP@CTAB synthesised in the 10 L reactor for a $HAuCl_4$ precursor concentration of 7.9 mM.

We analyzed the effect of the presence of silver nitrate. Colloidally stable seeds and particles enable higher precursor concentrations, and silver nitrate is known to affect the formation and stabilization of gold nanoparticles, which has been studied in detail for its effect on the formation of anisometric particles.[38-39] Starting from the Au4 sample, an increase of the silver nitrate concentration by a factor of 15 had no effect on the morphology of the particles

but reduced the average diameter to 54 nm with a standard deviation of 15 nm (Sample Au5, Figure 3B). The absence of $AgNO_3$ led to highly polydisperse particles, including a fraction in the micrometre range (Sample Au6, Figure 3C).

We used above results on the effects of the amount of seeds, and CTAB, sodium oleate and silver nitrate concentrations on particle quality at gold precursor concentrations of 4.6 mM to determine the maximum gold precursor concentrations that yields Au NPs with sizes below 100 nm and standard deviations below 15% at high yields. Increasing the $HAuCl_4 \cdot 3H_2O$ concentration up to 7.9 mM under the conditions used in sample Au5 with a proportional increase in the number of seeds and ascorbic acid and constant CTAB, sodium oleate, and silver nitrate concentrations produced particles with similar shape, an average diameter of 87 nm, and a standard deviation of 14 nm, slightly above that at lower concentrations (Sample Au7, Figure 3D). Increasing the gold precursor concentration to 12 mM resulted in polydisperse particles (Sample Au8, Figure 3E). We thus limited the gold precursor concentrations in all further experiments to a maximum of 7.9 mM.

All syntheses discussed above were performed without additional pH adjustments at pH ≅ 4.5 according to pH test strips. Adjusting the pH to 1 using 1 M HCl led to micrometric, polydisperse particles (not shown). Syntheses using the conditions of sample Au2 but carried out at temperatures of 25 and 30 ºC yielded NPs with similar features, but such lower temperatures caused some aggregation during the purification of the samples by centrifugation. We ascribe this to a reduced particle stabilization by CTAB, which is not soluble enough at such temperatures. An increase of CTAB and NaOL concentrations gave rise to viscous solutions that could not be analyzed further.

We found reaction yields from 88 to 92% for all syntheses at the 1 L scale after centrifugation from inductively coupled plasma optical emission spectrometry (ICP-OES). We ascribe the lossed to the centrifugation steps. Amounts up to 1.15 g of AuNP@CTAB per batch could thus be synthesised. The mean hydrodynamic particle diameters from DLS was

similar in all samples that contained monodisperse particles and consistent with the values from SEM/TEM. All synthesised AuNP@CTAB had ζ potentials of around +25 mV at pH 6.5, in good agreement with previous results.[3] We did not observe any reproducibilty issues in all the 1 L syntheses, which were carried out with the same 1 kg CTAB package.

3.2 Upscaling AuNP@CTAB synthesis at the 10 L scale

The experimental conditions found above for 1 L reactions were scaled to 10 L using a reactor with proportionally scaled geometry by increasing all absolute reactant amounts by the factor 10 as described in the experimental section. The reaction parameters that were optimal for the 1 L reactor could be used in the 10 L reactor, too, to obtain particles with comparable qualities. Syntheses in the 10 L reactor were performed for both 4.6 and 7.9 mM gold precursor concentrations, resulting in particles with the same morphology as in the corresponding 1 L batches. The homogeneity at lower gold concentrations was slightly better (sample Au9-10L, mean NPs size of 77 ± 8 nm, versus sample Au10-10L, Figure 3F, with a mean NPs size of 71 ± 29 nm). Reaction yields for the 10 L batches were around 85 - 90%, similar to those found in the 1 L reactions. The result of AuNP@CTAB was 6.50 and 11 g per batch after purification and centrifugation. Impurities in CTAB can differ for different suppliers or batches, which has been associated with reproducibility issues in the synthesis of gold nanoparticles.[39] We repeated the 10 L syntheses using two different 1 kg CTAB batches (details in section 2.1) and did not observe relevant changes in the particle morphology.

3.3 Formation mechanisms of AuNP@CTAB at high gold precursor concentrations

The scale-up results of above indicate that the slow and controlled addition of ascorbic acid, high CTAB concentrations, and small amounts of silver nitrate are required to obtain AuNP@CTAB with narrow size distributions even at high gold precursor concentrations. We hypothesize that such experimental conditions enhance the colloidal stability of both gold seeds and NPs, and that this is the key factor to obtain homogeneous NPs.

Different roles have been assigned to CTAB in the formation mechanisms of gold particles. A preferential CTAB absorption onto the lateral facets of gold nanoparticles[40] and the formation of elongated CTAB micelles that may act as a template[41] have been suggested reaction mechanisms for the synthesis of gold nanorods. Our experimental conditions lead to isometric NPs, and we suggest that the main role of CTAB in our synthesis is to prevent particle aggregation. Silver in different states has been found on the surface gold particles,[42,43] both as CTAB-silver bromide complex[44] and as adsorbed $AgBr^{2-}$ species.[45] Monolayers or submonolayers of Ag(0) on the gold nanoparticles have also been reported.[38] The evolution of the surface plasmon resonance band of the gold seeds in our syntheses with Ag (I) are compatible with the presence of silver species on the seeds´ surfaces (Figure S2). Moreover, energy-dispersive X-ray (EDX) spectra indicated the presence of silver on the final AuNP@PEDOT:PSS (Figure S3). We hypothesize that such silver species, either Ag (0) or CTAB-silver bromide or $AgBr^{2-}$, help prevent seed and nanoparticle aggregation, especially for higher gold precursor concentrations, and modulate the deposition of the reduced gold cations onto the seed surface.

We propose a formation and growth mechanism as sketched in Figure 4. The gold seeds were colloidally unstable when no silver was added even in presence of large CTAB concentrations. This caused seed and particle aggregation. The deposition of gold on aggregates after the addition of ascorbic acid led to the formation of larger and polydisperse particles (Sample Au6, Figure 3C). Higher concentration of silver nitrate gave rise to more stable seeds, strongly minimized the seed aggregation and thus increased the final global number of seeds, which is associated with a smaller gold particle size (Sample Au5, Figure 3B). This is similar to the synthesis of spherical citrate-capped gold NPs,[24] which can be considered as a seed-grow mediated mechanism at least at high citrate concentrations.[46]

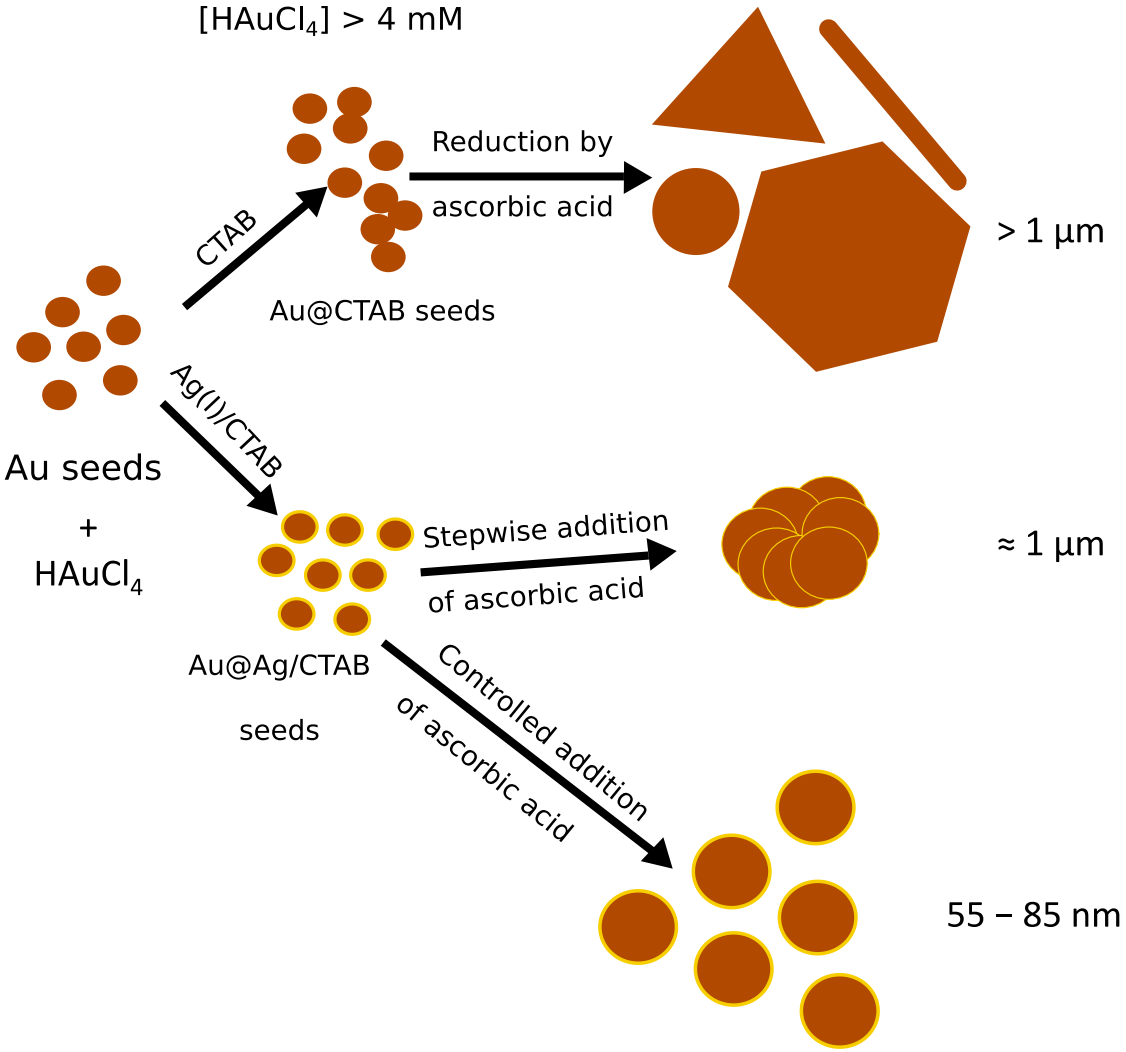

Figure 4: Reaction mechanism proposed for the formation of gold nanoparticles at increased $HAuCl_4$ concentrations (>4 mM). Ascorbic acid reduces the gold precursor, which is then deposited onto the seed surface and gives rise to particle growth. In absence of silver nitrate, the way ascorbic acid is added to the reaction system did not affect the final morphology of the particles.

3.4 Surface modification by ligand exchange with PEDOT:PSS

The CTAB-capped particles were colloidally stable when stored at room temperature in a CTAB solution but not in pure water.[47] We dispersed all AuNP@CTAB in 5 mM CTAB

solution. We removed the sacrificial CTAB ligand in a ligand exchange process with the conductive polymer PEDOT:PSS and made sure to avoid particle aggregation or reshaping.

A full batch of AuNP@CTAB was incubated in an aqueous solution of PEDOT:PSS in the 10 L reactor (reaction volume 8250 mL) as illustrated for the Au9-10L sample in the following. A mass ratio of 1:0.8 was chosen for AuNP@CTAB:PEDOT:PSS in order to form a sufficiently dense polymer ligand layer around the Au NPs. The residual CTAB concentration was 80 µM. The same values have been optimized and reported in previous work at a batch size of 10 mL.[3] After ligand exchange, the sample was purified by centrifugation, filtered, and dispersed in 27 mL of Millipore water at a final gold concentration of 200 mg /mL (Sample Au9-10L-LE, Table 1, Figure 5A).

A charge reversal of the nanoparticle surfaces (ζ potential changed from +25 to -40 mV at pH 6.5) was observed in good agreement with previous studies at the laboratory scale,[3] as well as very slight shift in the maximum of the gold surface plasmon resonance band (Figure S4). The resulting AuNP@PEDOT:PSS particles were free of aggregation according to DLS (Z average hydrodynamic diameter of 82 nm, Figure 5B, red line, with almost no changes when compared to the original AuNP@CTAB sample Au9-10L, black line, with a value of 80 nm). The total reaction yield in terms of gold after ligand exchange and all the centrifugation steps was around 83%, and 75% after filtering with a 1.5 µm filter.

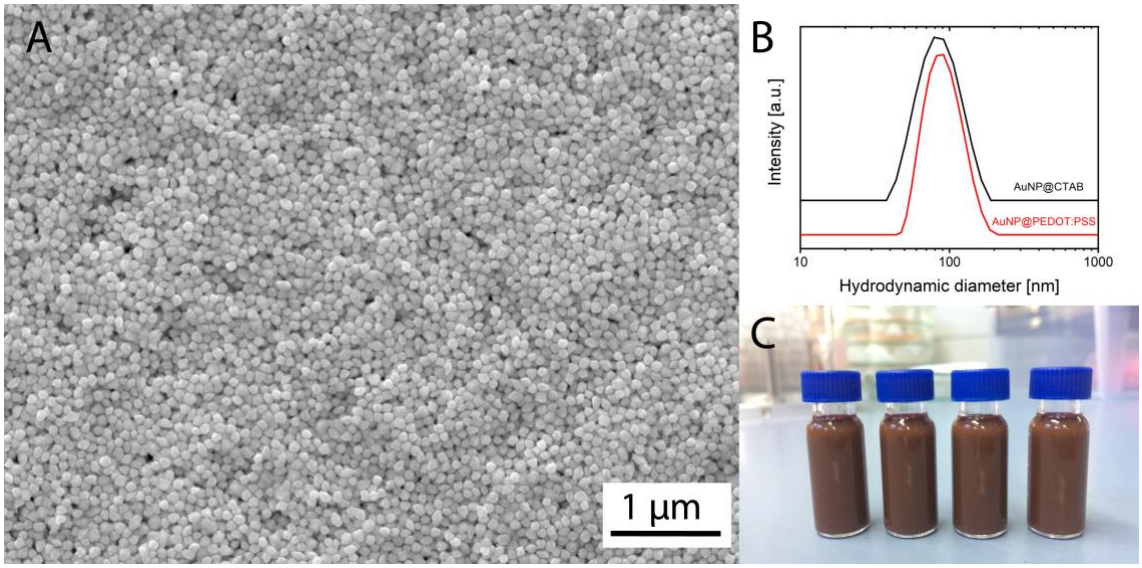

Figure 5: (A) Scanning electron (SEM) micrograph of Au NPs synthesised in a 10 L reactor after ligand exchange with PEDOT:PSS (sample Au9-10L-LE). The particle morphology remained unchanged. (B) Hydrodynamic diameter from DLS for the initial Au9-10L sample (AuNP@CTAB, black line) and the same particles after ligand exchange (Sample Au9-10L-LE, AuNP@PEDOT:PSS, red line), indicating good dispersion. (C) Final aqueous dispersions of hybrid AuNP@PEDOT:PSS with a gold concentration of 200 mg/mL suitable for inkjet printing.

3.5 Inkjet printing of hybrid AuNP@PEDOT:PSS

We demonstrated the quality and printability of the hybrid NPs from 10 L-scale synthesis using an inkjet printer to print conductive paths on different substrates. Inkjet printing requires sufficient ink volume to fill the cartridge and print the desired patterns. The particles have to be sufficiently small to pass though the nozzle (21.5 µm diameter)[48] and should not contain residual larger objects that would clog it. Excellent colloidal stability is required for long-term storage of the inks and to ensure homogeneous deposited layers.

We increased the gold concentration of sample Au9-10L-LE to 200 mg/mL using centrifugation as described in the experimental section. The resulting dispersion (Figure

5C) had a density of 1.19 mg/mL, a surface tension (γ) of 54.1 ± 1.1 mN m^{-1}, and a viscosity of 9 cP. Note that other polar solvents such as alcohols and acetone can be used as a solvent without agglomeration of the particle according to previous reports.[3] The above-mentioned formulation in water had an Ohnesorge (Oh) number of 0.24 for a nozzle diameter of 21.5 μm (10 pL nozzle from Dimatix's cartridge) which is in the range required for stable printing.[49]

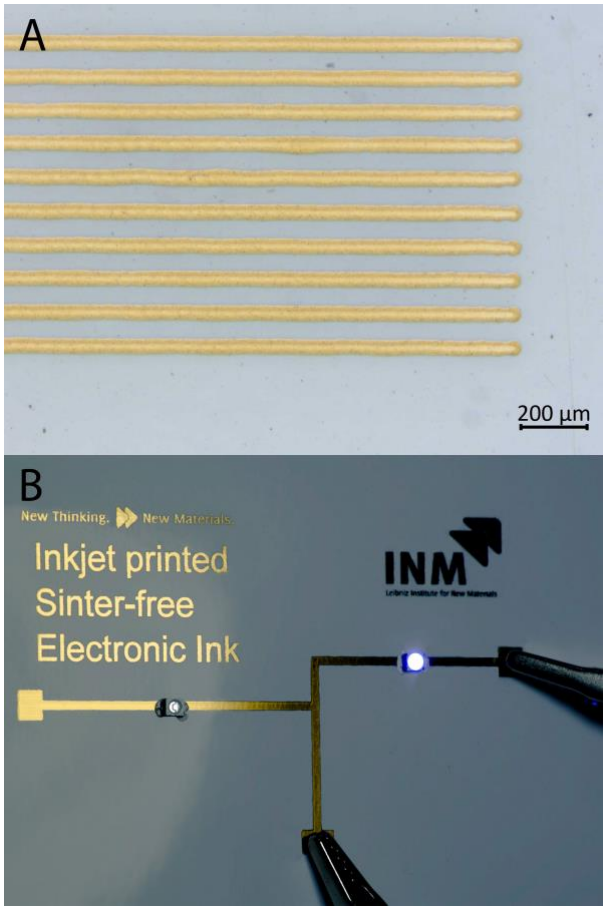

Figure 6: (A) Conductive lines of hybrid AuNP@PEDOT:PSS inkjet printed with the PiXDRO LP50 printer on PET foils. (B) Conductive structures printed on paper using a commodity Epson - WF-2010W inkjet printer. A commercial LED was attached to the circuit with silver paste (ACHESON Silver DAG 1415, Plano GmbH, Wetzlar, Germany). Copyright logo: INM.

Hybrid NP suspensions from the scaled synthesis were inkjet printed onto a large variety of substrates, including paper, cardboard, polymer foils, silicone, glass, and ceramics. In some of the cases, a pre-treatment of the substrate with oxygen plasma for 4 minutes was used to enhance the wettability of the substrate. The printed patterns became conductive upon drying (see Supporting Information). The achievable resolution depended on the inkjet printer and substrate; in the case of a PiXDRO LP50 printer with a Dimatix printhead, conductive lines with widths of 40 μm and moderate line edge roughness were routinely obtained on PET (Figure 6A). The sinter-free ink is also suitable for standard commodity printers as shown in a print on paper in Figure 6B. The resulting AuNP@PEDOT:PSS remained stable in storage; they were printable and formed conductive layers for at least 6 months after their synthesis.

The electrical properties of the printed patterns were measured using 9 lines of approximately 1.5 cm length and 1 mm width that we printed on glass. The cross-sectional area perpendicular to the long axis was estimated from the profiles recorded by confocal microscopy. The electrical resistance (R) of the samples was measured using 2-point-probe and the volumetric resistivity (ρ) calculated as described in the experimental section. The average resistivity of the patterns printed with the sinter-free ink was $4.42 \cdot 10^{-5} \pm 7.57 \cdot 10^{-6}$ Ω m some minutes after printing. It dropped to values in a range of 25 to 55 % (36% on average) after 24 h of drying at room temperature. One should notice that drying times generally depend on the relative humidity, temperature, and substrate.[50]

4. Conclusions

The synthesis of hybrid nanoparticles with gold cores and conductive polymer shells was scaled to 10 L batches and optimized to yield gram-scale amounts of functional hybrid nanoparticles per batch. We modified concentrations, addition rates, temperatures, and purification protocols to obtain well-dispersed particles. The maximum particle density of

the product was limited by the trade-off between a narrow size distribution in the desired range and the agglomeration of particles at different stages.

Conductive polymers are expensive and cannot be recovered from the reaction mixture. It is not economical to use the conductive polymer directly in particle synthesis given the small particle concentrations. We therefore used a "sacrificial ligand" approach and prepared the particles using CTAB, a low-cost reagent that is able to control the morphology of the particles even at relatively high precursor concentrations. The disadvantage of this approach is the limited colloidal stability of CTAB-coated AuNP that requires considerable care in downstream processing.

Amounts of 10 g of dry AuNP@CTAB were obtained in single batches using a 10 L reactor. Slow and controlled addition of ascorbic acid and the presence of small amounts of $AgNO_3$ were found as key variables to obtain nanoparticles with narrow size distributions with an average that could be tuned between 54 to 85 nm by adjusting the reagent concentrations.

The sacrifical CTAB ligand was replaced by PEDOT:PSS in a second step at room temperature with a 1:0.8 AuNP@CTAB : PEDOT:PSS mass ratio and a residual CTAB concentration of 80 μm, as demonstrated by a charge reversal of the particle surface. No particle aggregation or reshaping was observed, and the the functional PEDOT:PSS ligand provided the nanoparticles with high colloidal stability at high nanoparticle concentrations (200 mg NPs / mL). Quality and stability were sufficient to prepare concentrated aqueous dispersions which could be deposited via inkjet printing onto a variety of substrates, giving rise to conductive circuits and structures at room temperature with no further treatment.

The sacrificial ligand strategy is a scalable approach that can be extended to surfactants beyond CTAB and is suitable for the scale-up of various hybrid nanoparticle syntheses. Several surfactants have been shown to direct the shape of metal, semiconductor and oxide nanoparticles; we did not exploit the shape-directing capabilities of CTAB beyond size control in this work but note in passing that gold nanorods are now commercially prepared

using CTAB as directing agent. The strategy is compatible with other rector concepts such as the continuous stirred-tank (CSTR) and other continuous approaches that are suitable to produce larger particle quantities while retaining the relatively low particle concentration.

5. Acknowledgements

The authors would like to thank Prof. Dr. Eduard Arzt for his continuing support of the project. Dr. Marcus Koch is thanked for help with EDX measurements, and Ms. María Rodríguez for her assistance in the preparation of some of the samples. Funding from the German Federal Ministry of Education and Research in the "NanoMatFutur" program is gratefully acknowledged. A.E. also acknowledges the support of the sixth Research and Technology Transfer Plan of the University of Seville (VI PPIT- US).

6. **Supporting Information**

The Supporting Information is available free of charge at XXXXX

- Images of the reactors and EDX and UV-VIS spectra of samples.

References

1. Benelmekki, M., Designing Hybrid Nanoparticles. Morgan & Claypool Publishers: 2015.
2. Heuer-Jungemann, A.; Feliu, N.; Bakaimi, I.; Hamaly, M.; Alkilany, A.; Chakraborty, I.; Masood, A.; Casula, M. F.; Kostopoulou, A.; Oh, E.; Susumu, K.; Stewart, M. H.; Medintz, I. L.; Stratakis, E.; Parak, W. J.; Kanaras, A. G., The Role of Ligands in the Chemical Synthesis and Applications of Inorganic Nanoparticles. *Chem. Rev.* **2019,** *119*, 4819-4880.
3. Reiser, B.; González-García, L.; Kanelidis, I.; Maurer, J. H. M.; Kraus, T., Gold nanorods with conjugated polymer ligands: sintering-free conductive inks for printed electronics. *Chem. Sci.* **2016,** *7*, 4190-4196.
4. Hood, M. A.; Mari, M.; Muñoz-Espí, R., Synthetic Strategies in the Preparation of Polymer/Inorganic Hybrid Nanoparticles. *Materials* **2014,** *7*, 4057-4087.
5. Escudero, A.; Carrillo-Carrión, C.; Romero-Ben, E.; Franco, A.; Rosales-Barrios, C.; Castillejos, M. C.; Khiar, N., Molecular Bottom-Up Approaches for the Synthesis of Inorganic and Hybrid Nanostructures. *Inorganics* **2021,** *9*, 58.
6. Chang, H.-H.; Murphy, C. J., Mini Gold Nanorods with Tunable Plasmonic Peaks beyond 1000 nm. *Chem. Mat.* **2018,** *30*, 1427-1435.
7. Kozek, K. A.; Kozek, K. M.; Wu, W.-C.; Mishra, S. R.; Tracy, J. B., Large-Scale Synthesis of Gold Nanorods through Continuous Secondary Growth. *Chem. Mat.* **2013,** *25*, 4537-4544.
8. Park, K.; Drummy, L. F.; Wadams, R. C.; Koerner, H.; Nepal, D.; Fabris, L.; Vaia, R. A., Growth Mechanism of Gold Nanorods. *Chem. Mat.* **2013,** *25*, 555-563.
9. Silvert, P.-Y.; Herrera-Urbina, R.; Duvauchelle, N.; Vijayakrishnan, V.; Elhsissen, K. T., Preparation of colloidal silver dispersions by the polyol process. Part 1—Synthesis and characterization. *J. Mater. Chem.* **1996,** *6*, 573-577.
10. Hokita, Y.; Kanzaki, M.; Sugiyama, T.; Arakawa, R.; Kawasaki, H., High-Concentration Synthesis of Sub-10-nm Copper Nanoparticles for Application to Conductive Nanoinks. *ACS Appl. Mater. Interfaces* **2015,** *7*, 19382-19389.
11. Hiramatsu, H.; Osterloh, F. E., A Simple Large-Scale Synthesis of Nearly Monodisperse Gold and Silver Nanoparticles with Adjustable Sizes and with Exchangeable Surfactants. *Chem. Mat.* **2004,** *16*, 2509-2511.
12. Ye, X.; Jin, L.; Caglayan, H.; Chen, J.; Xing, G.; Zheng, C.; Doan-Nguyen, V.; Kang, Y.; Engheta, N.; Kagan, C. R.; Murray, C. B., Improved Size-Tunable Synthesis of Monodisperse Gold Nanorods through the Use of Aromatic Additives. *ACS Nano* **2012,** *6*, 2804-2817.
13. Guerrini, L.; Alvarez-Puebla, R. A.; Pazos-Perez, N., Surface Modifications of Nanoparticles for Stability in Biological Fluids. *Materials* **2018,** *11*, 1154.
14. Hühn, J.; Carrillo-Carrion, C.; Soliman, M. G.; Pfeiffer, C.; Valdeperez, D.; Masood, A.; Chakraborty, I.; Zhu, L.; Gallego, M.; Yue, Z.; Carril, M.; Feliu, N.; Escudero, A.; Alkilany, A. M.; Pelaz, B.; del Pino, P.; Parak, W. J., Selected Standard Protocols for the Synthesis, Phase Transfer, and Characterization of Inorganic Colloidal Nanoparticles. *Chem. Mat.* **2017,** *29*, 399-461.
15. Wu, S.-H.; Chen, D.-H., Synthesis of high-concentration Cu nanoparticles in aqueous CTAB solutions. *J. Colloid Interface Sci.* **2004,** *273*, 165-169.
16. Dewi, M. R.; Laufersky, G.; Nann, T., A highly efficient ligand exchange reaction on gold nanoparticles: preserving their size, shape and colloidal stability. *RSC Adv.* **2014,** *4*, 34217-34220.
17. Indrasekara, A. S. D. S.; Wadams, R. C.; Fabris, L., Ligand Exchange on Gold Nanorods: Going Back to the Future. *Part. Part. Syst. Charact.* **2014,** *31*, 819-838.
18. Thierry, B.; Ng, J.; Krieg, T.; Griesser, H. J., A robust procedure for the functionalization of gold nanorods and noble metal nanoparticles. *Chem. Commun.* **2009**, 1724-1726.

19. Nayak, L.; Mohanty, S.; Nayak, S. K.; Ramadoss, A., A review on inkjet printing of nanoparticle inks for flexible electronics. *J. Mater. Chem. C* **2019,** *7*, 8771-8795.
20. Ye, X.; Zheng, C.; Chen, J.; Gao, Y.; Murray, C. B., Using Binary Surfactant Mixtures To Simultaneously Improve the Dimensional Tunability and Monodispersity in the Seeded Growth of Gold Nanorods. *Nano Lett.* **2013,** *13*, 765-771.
21. Tebbe, M.; Kuttner, C.; Männel, M.; Fery, A.; Chanana, M., Colloidally Stable and Surfactant-Free Protein-Coated Gold Nanorods in Biological Media. *ACS Appl. Mater. Interfaces* **2015,** *7*, 5984-5991.
22. Nikoobakht, B.; El-Sayed, M. A., Preparation and Growth Mechanism of Gold Nanorods (NRs) Using Seed-Mediated Growth Method. *Chem. Mat.* **2003,** *15*, 1957-1962.
23. Jana, N. R.; Gearheart, L.; Murphy, C. J., Wet Chemical Synthesis of High Aspect Ratio Cylindrical Gold Nanorods. *J. Phys. Chem. B* **2001,** *105*, 4065-4067.
24. Wuithschick, M.; Birnbaum, A.; Witte, S.; Sztucki, M.; Vainio, U.; Pinna, N.; Rademann, K.; Emmerling, F.; Kraehnert, R.; Polte, J., Turkevich in New Robes: Key Questions Answered for the Most Common Gold Nanoparticle Synthesis. *ACS Nano* **2015,** *9*, 7052-7071.
25. Tighe, C. J.; Cabrera, R. Q.; Gruar, R. I.; Darr, J. A., Scale Up Production of Nanoparticles: Continuous Supercritical Water Synthesis of Ce–Zn Oxides. *Ind. Eng. Chem. Res.* **2013,** *52*, 5522-5528.
26. Spoljaric, S.; Ju, Y.; Caruso, F., Protocols for Reproducible, Increased-Scale Synthesis of Engineered Particles—Bridging the "Upscaling Gap". *Chem. Mat.* **2021,** *33*, 1099-1115.
27. Scarabelli, L.; Sánchez-Iglesias, A.; Pérez-Juste, J.; Liz-Marzán, L. M., A "Tips and Tricks" Practical Guide to the Synthesis of Gold Nanorods. *J. Phys. Chem. Lett.* **2015,** *6*, 4270-4279.
28. Gou, L.; Murphy, C. J., Fine-Tuning the Shape of Gold Nanorods. *Chem. Mat.* **2005,** *17*, 3668-3672.
29. Keul, H. A.; Möller, M.; Bockstaller, M. R., Structural Evolution of Gold Nanorods during Controlled Secondary Growth. *Langmuir* **2007,** *23*, 10307-10315.
30. Sau, T. K.; Murphy, C. J., Room Temperature, High-Yield Synthesis of Multiple Shapes of Gold Nanoparticles in Aqueous Solution. *J. Am. Chem. Soc.* **2004,** *126*, 8648-8649.
31. Wang, Y.; Teitel, S.; Dellago, C., Surface-Driven Bulk Reorganization of Gold Nanorods. *Nano Lett.* **2005,** *5*, 2174-2178.
32. Park, K.; Hsiao, M.-s.; Yi, Y.-J.; Izor, S.; Koerner, H.; Jawaid, A.; Vaia, R. A., Highly Concentrated Seed-Mediated Synthesis of Monodispersed Gold Nanorods. *ACS Appl. Mater. Interfaces* **2017,** *9*, 26363-26371.
33. Matijevic, E., Preparation and properties of uniform size colloids. *Chem. Mat.* **1993,** *5*, 412-426.
34. Escudero, A.; Becerro, A. I.; Carrillo-Carrion, C.; Núñez, N.; Zyuzin, M. V.; Laguna, M.; González-Mancebo, D.; Ocaña, M.; Parak, W. J., Rare earth based nanostructured materials: synthesis, functionalization, properties and bioimaging and biosensing applications. *Nanophotonics* **2017,** *6*, 881-921.
35. Jia, H.; Fang, C.; Zhu, X.-M.; Ruan, Q.; Wang, Y.-X. J.; Wang, J., Synthesis of Absorption-Dominant Small Gold Nanorods and Their Plasmonic Properties. *Langmuir* **2015,** *31*, 7418-7426.
36. Perrault, S. D.; Chan, W. C. W., Synthesis and Surface Modification of Highly Monodispersed, Spherical Gold Nanoparticles of 50−200 nm. *J. Am. Chem. Soc.* **2009,** *131*, 17042-17043.
37. Jana, N. R.; Gearheart, L.; Murphy, C. J., Evidence for Seed-Mediated Nucleation in the Chemical Reduction of Gold Salts to Gold Nanoparticles. *Chem. Mat.* **2001,** *13*, 2313-2322.
38. Liu, M.; Guyot-Sionnest, P., Mechanism of Silver(I)-Assisted Growth of Gold Nanorods and Bipyramids. *J. Phys. Chem. B* **2005,** *109*, 22192-22200.

39. Jessl, S.; Tebbe, M.; Guerrini, L.; Fery, A.; Alvarez-Puebla, R. A.; Pazos-Perez, N., Silver-Assisted Synthesis of Gold Nanorods: the Relation between Silver Additive and Iodide Impurities. *Small* **2018,** *14*, 1703879.
40. Murphy, C. J.; Sau, T. K.; Gole, A. M.; Orendorff, C. J.; Gao, J.; Gou, L.; Hunyadi, S. E.; Li, T., Anisotropic Metal Nanoparticles: Synthesis, Assembly, and Optical Applications. *J. Phys. Chem. B* **2005,** *109*, 13857-13870.
41. Jana, N. R., Gram-Scale Synthesis of Soluble, Near-Monodisperse Gold Nanorods and Other Anisotropic Nanoparticles. *Small* **2005,** *1*, 875-882.
42. Wang, Y.; Aili, D.; Selegård, R.; Tay, Y.; Baltzer, L.; Zhang, H.; Liedberg, B., Specific functionalization of CTAB stabilized anisotropic gold nanoparticles with polypeptides for folding-mediated self-assembly. *J. Mater. Chem.* **2012,** *22*, 20368-20373.
43. Backes, I. K.; González-García, L.; Holtsch, A.; Müller, F.; Jacobs, K.; Kraus, T., Molecular Origin of Electrical Conductivity in Gold–Polythiophene Hybrid Particle Films. *J. Phys. Chem. Lett.* **2020,** *11*, 10538-10547.
44. Hubert, F.; Testard, F.; Spalla, O., Cetyltrimethylammonium Bromide Silver Bromide Complex as the Capping Agent of Gold Nanorods. *Langmuir* **2008,** *24*, 9219-9222.
45. Niidome, Y.; Nakamura, Y.; Honda, K.; Akiyama, Y.; Nishioka, K.; Kawasaki, H.; Nakashima, N., Characterization of silver ions adsorbed on gold nanorods: surface analysis by using surface-assisted laser desorption/ionization time-of-flight mass spectrometry. *Chem. Commun.* **2009**, 1754-1756.
46. Chow, M. K.; Zukoski, C. F., Gold Sol Formation Mechanisms: Role of Colloidal Stability. *J. Colloid Interface Sci.* **1994,** *165*, 97-109.
47. Barbero, F.; Moriones, O. H.; Bastús, N. G.; Puntes, V., Dynamic Equilibrium in the Cetyltrimethylammonium Bromide–Au Nanoparticle Bilayer, and the Consequent Impact on the Formation of the Nanoparticle Protein Corona. *Bioconjugate Chem.* **2019,** *30*, 2917-2930.
48. Kamyshny, A.; Magdassi, S., Conductive Nanomaterials for Printed Electronics. *Small* **2014,** *10*, 3515-3535.
49. Brian, D., Inkjet Printing of Functional and Structural Materials: Fluid Property Requirements, Feature Stability, and Resolution. *Ann. Rev. Mater. Res.* **2010,** *40*, 395-414.
50. Kang, D. J.; Jüttke, Y.; González-García, L.; Escudero, A.; Haft, M.; Kraus, T., Reversible Conductive Inkjet Printing of Healable and Recyclable Electrodes on Cardboard and Paper. *Small* **2020,** *16*, 2000928.